DETECTION AND IMAGING OF DEFECTS ESPECIALLY MATERIALS WITH SMALL UT TRANSDUCERS USING BROAD-BAND HOLOGRAPHY

L. V. Bernus, M. Kroning, and J. Regn
Siemens AG, KWU Group
Hammerbacher Str. 12 + 14
8520 Erlangen, West Germany

H. Ermert, Ruhr-Universitat Bochum
Inst. f. Hoch- und Hochstfrequenztechnik
4630 Bochum, West Germany

G. Prokoph, Universitat Erlangen-Nurnberg
Inst. f. Hochfrequenztechnik
Cauerstr. 9
8520 Erlangen, West Germany

INTRODUCTION

Since conventional single frequency acoustical holography provides only poor axial resolution, this concept was improved with the multifrequency holography to enhance the imaging quality. This leads to long data acquisition times because of the need to measure each frequency. A further step towards a fast imaging system with good spatial resolution is broadband holography. Here, one illuminates the object with broadband signals in a single measurement procedure.

THEORETICAL PRINCIPLES

Broadband holography is based on the same theoretical principles as the multi-frequency holography, and these principles are discussed below. The respective geometrical relations are shown in Figure 1. The ultrasonic signal f_B of a transducer located at the position $(x_B, 0)$ is reflected by a scatterer P and received by a receiver at a point x_A within the aperture. The signal of the transducer and that of the receiver f_{rec} can be represented in the frequency domain. An image function B is defined as follows:

$$B(\chi, z) = \left| \int_{\chi_A} \int_{\omega} F_{rec}(\chi_A, \omega) F^{*}_{LS}(\chi_A, \omega, \chi, z) d\omega d\chi_A \right| \qquad (1)$$

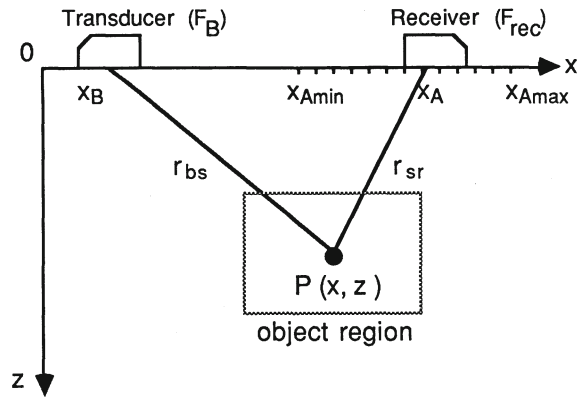

Fig. 1. Geometrical relations for the bistatic case.

The received signals F_{rec} are compared with calculated signals F_{LS}, which would be recorded at a position x_A if there was an isolated line scatterer at the position (x, z). B (x, z) represents the intensity of a certain pixel in the corresponding image. The signals F_{LS} can be regarded as a filtered and time delayed version of the transmitted waveform;

$$F_{LS}(x_A, \omega, x, z) = F_B(\omega) H(\omega) \frac{e^{i\omega\tau_l(x_A, x, z)}}{\sqrt{\tau_{bs}\tau_{sr}}} \tag{2}$$

$H(\omega)$ is the system transfer function F_B is the transducer signal and τ_l represents the time of flight from the transmitter to the receiver and depends on the actual geometrical situation.

Introducing a modified received signal F'_{rec} given as

$$F'_{rec}(x_A, \omega) = F_{rec}(x_A, \omega) F^*_B(\omega) H^*(\omega) \tag{3}$$

one obtains for the image function B (x, z):

$$B(x, z) = \left| \int_{x_a} \int_{\omega} F'_{rec}(x_A, \omega) \frac{e^{i\omega\tau_l}}{\sqrt{\tau_{bs}\tau_s\tau}} d\omega dx_A \right| \tag{4}$$

Performing the integration by w one gets

$$B(x, z) = \left| \int_{x_A} f'_{rec}(x_A, \tau_l) \frac{1}{\sqrt{\tau_{bs}\tau_s\tau}} dx_a \right| \tag{5}$$

F_{rec} in the time domain is given by

$$f'_{rec}(x_A, t) = f_B(-t) * h(-t) * (f_{rec}(x_A, t) + iHI(f_{rec}(x_A, t))) \tag{6}$$

where HI denotes the Hilbert Transformation by which one gets the imaginary part of the received signal. Neglecting the geometrical factor for small objects far from the aperture one comes to the following equation which is similar to the SAFT reconstruction formula,

$$B(x, z) = \left| \int_{x_A} f'_{rec}(x_A, \tau_l) dx_A \right| \tag{7}$$

For discrete aperture positions the integration over the aperture changes into a summation,

$$B(x,z)=\left|\sum_{j=1}^{N} f'_{rec}(x_A,\tau_i(j))\right|. \quad (8)$$

Here, n is the number of aperture points.

Therefore the reconstruction process can be regarded as the summation of the complex-valued and filtered A-scans according to their times of flight. In Figure 2 a comparison between a holographic and SAFT-reconstruction is shown. It turns out that a broadband holography algorithm produces a very clear image of the five line scatterers, while there are oscillations using the SAFT procedure because of RF-data being summed. These oscillations can be removed by forming an imaginary part of the data and imaging the absolute value.

As mentioned it is necessary for the reconstruction to form modified received signals by a linear filter operation and by adding the imaging part. Here the filtering process is included in the generation of the transmitted waveform using a function synthesizer to generate arbitrary waveforms, in order to save time in the numerical reconstruction process. If an optimum axial resolution is desired the transmitted signal should be chosen for the shortest echoes possible. That leads to the concept of inverse filtering. To calculate the transmitted waveform desired, knowledge of system transfer function and appropriate windowing is necessary. Here, the windowing is performed using a trunctuated cosine. The resulting signal using inverse filtering is shown in Figure 3. It is obvious that a considerable reduction of echo signal duration is achieved.

RESOLUTION

Regarding the approximated line spread function for a single line scatterer, one can get a measure for the axial and lateral resolution of the system. A small aperture and a small object area are assumed. For the axial resolution one gets for the full width at half maximum of the line spread function:

$$\delta_a=\frac{c}{\Delta f}. \quad (9)$$

That means that the resolution decreases with a smaller bandwidth Δ, f, where c is the sound velocity

$$\delta_l=f(\Delta f)\frac{\lambda_m r_0}{D\cos\beta_0} \quad (10)$$

The full width at half maximum for the line spread function in lateral direction is given by

$$\delta_l=f(\Delta f) \quad (10)$$

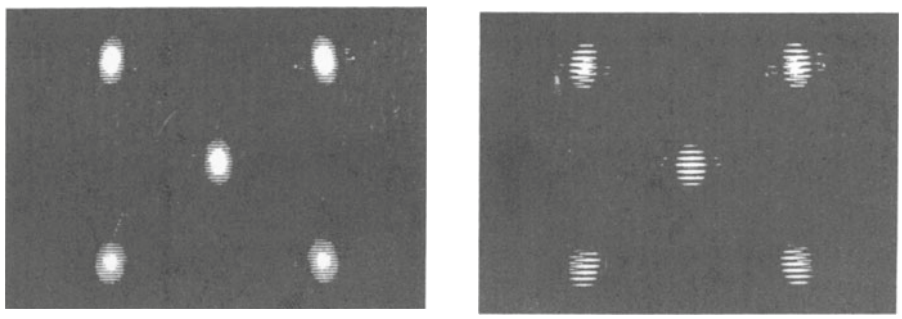

Fig. 2. Comparison between a holographic (left hand side) and a SAFT (right hand side) reconstruction.

where the point scatterer is located at a point $(r_o \sin\beta_o, r_o \cos\beta_o)$. f is a factor with a weak dependence of the bandwidth and λ_m is the center wavelength. The result is that the lateral resolution decreases with the width of the aperture D and the center frequency. These results derived for the monostatic case are also transferable to the bistatic case where the axial resolution remains unchanged, and the lateral resolution is reduced by a factor of two.

IMAGE DETERIORATION DUE TO ERRORS IN THE RECEIVED SIGNALS

Simulations of errors in the received signals show the following effects on the reconstructed images:

1) electronic noise, which was supposed to be purely statistical, produces noise in the image, however with a small amplitude due to the intrinsic summation of the signals in the reconstruction algorithm;
2) a small constant time offset moves the image function in the axial direction. A large constant time offset causes a smearing in the lateral direction, too;
3) a small error in the sound velocity causes the image function to be moved in axial and lateral directions. Larger errors result in an additional smearing of the image function;
4) weak inhomogeneous materials act like statistical noise and provide light smearing in the image. A reconstruction fails for strongly inhomogeneous materials because no more constructive superposition of the real echoes is possible. Multiple scattering leads to artifacts in the image but with intensities lower than those of the scatterers because multiple scattering is not a completely statistical process.

EXPERIMENTAL RESULTS

Examples of reconstructions with measured data are shown in this section to point out the properties of the broadband holography reconstruction algorithm. In Figure 4, a reconstruction of a test block with four cylindrical holes is shown. The diameter of each hole was 2 mm; the size of the object area was 20 mm x 30 mm. The artifacts in the reconstructed image are due to multiple scattering and mode conversion processes. These artifacts having a small amplitude the four holes are well resolved with a reasonably good intensity.

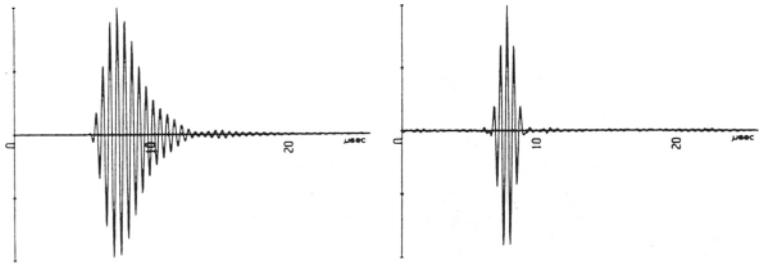

Measured impulse response

Measured response to an optimized excitation (inverse filtering)

Fig. 3. Measured received Signal without (lhs.) and with (rhs.) inverse filtering.

The next example is shown in Figure 5. It is a natural flaw in a test block. The size of the object area was 70 mm x 70 mm. Here the size of the flaw can clearly be recognized. Another example is the reconstruction of a natural defect in austenitic steel shown in Figure 6. The two A-scans in Figure 7 belong to the numbered aperture positions in the schematic view of the test arrangement. The signal of the defect should appear at the marked positions in the A-scans, but it is superimposed on noise. In the reconstruction, however, the defect can clearly be recognized.

CONCLUSIONS

Using broadband holography one gets short data acquisition times, performing only one measurement per sampling point. The reconstruction is performed in time-domain with pre-filtered complex signals which are summed according to their times of flight, including a geometrical factor if necessary. The image is achieved by taking the absolute value of the summed signals. The reconstruction algorithm provides both a good axial and a good lateral resolution. Interference can be suppressed by using a large bandwidth. By using analytical signals with a real and an imaginary part the image function will not contain oscillations. Because of the summation of these analytical signals, noisy signals can be tolerated. Even signals from highly textured materials produce only slightly disturbed images.

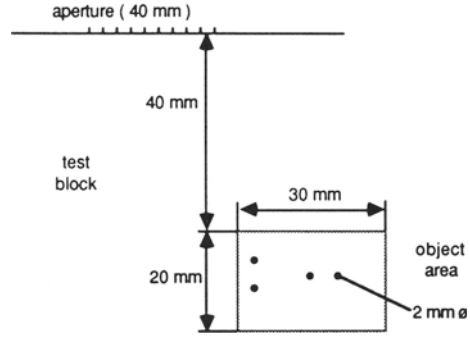

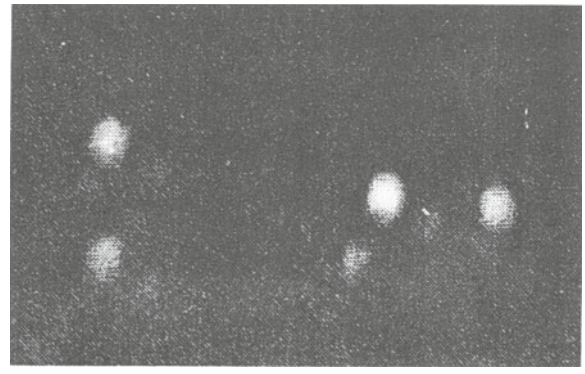

Fig. 4. Schematic view (upper image) and reconstruction (lower image) of a test block with four cylindrical holes. Aperture: 40 mm (121 Sampling points), frequency: 1.5-3.5 MHz, sound velocity: 3.23 mm/μs.

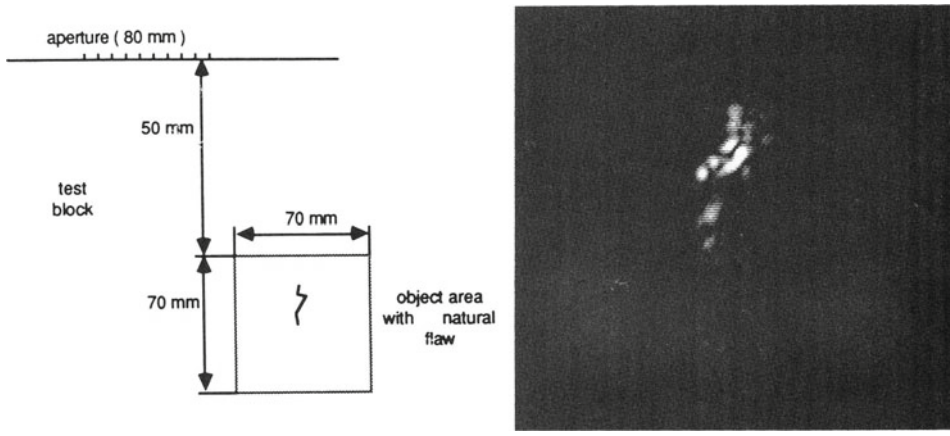

Fig. 5. Schematic view (lhs.) and reconstruction (rhs.) of a test block with a natural flaw. Aperture 80 mm (161 Sampling points), frequency: 1.5-3.5 MHz, sound velocity: 3.23 mm/μs.

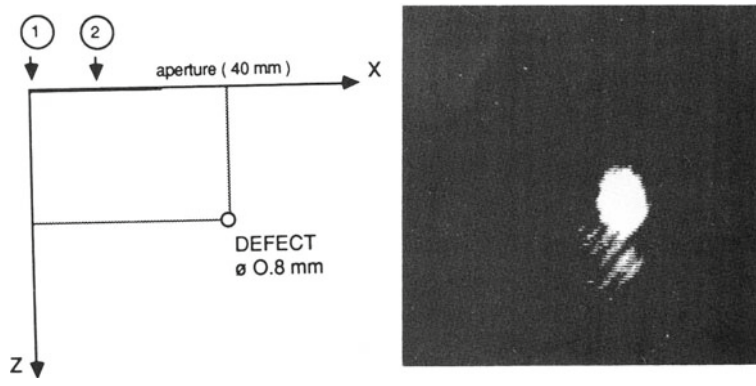

Fig. 6. Schematic view (lhs.) and reconstruction (rhs.) of a natural defect in austenitic steel. Aperture: 40 mm (41 Sampling points), frequency: 1.8-3.8 MHz, sound velocity: 5.9 mm/μs.

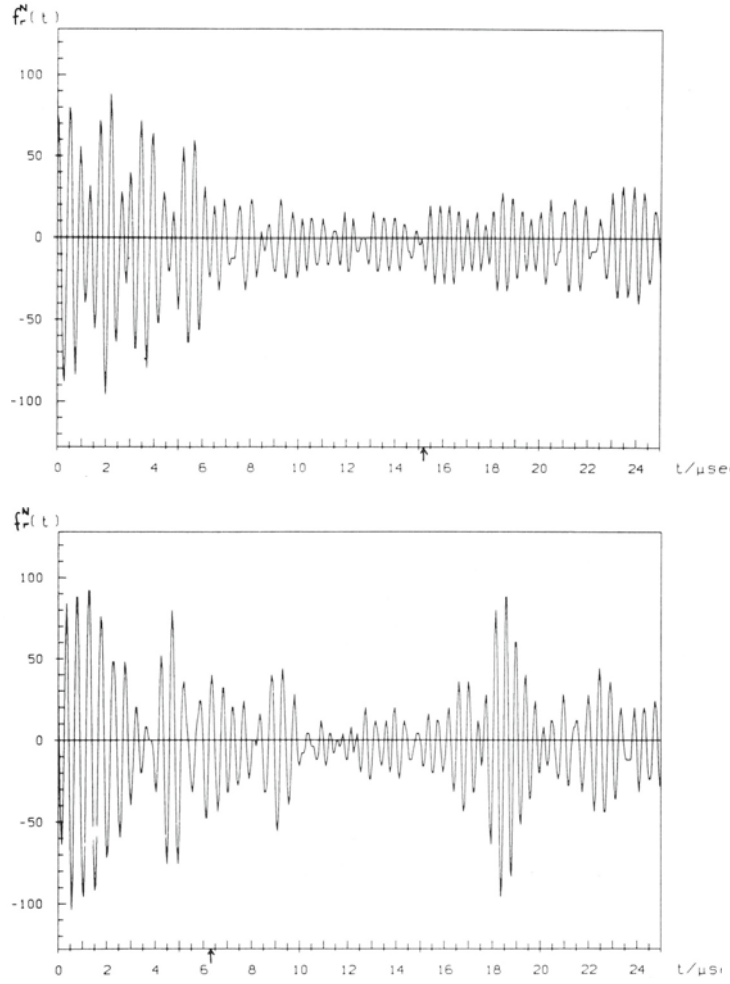

Fig. 7. A-scans of the marked aperture points (1-upper image and 2-lower image of Fig. 6). The expected position of the defect is indicated by arrows.

REFERENCES

1. M. Ahmed, K. Wang, A. Metherell: Holography and Its Applications to Acoustic Imaging, Proc. IEEE, vol. 67 (1979).
2. J. Kutzner, H. Wustenberg: Akustische Linienholographie, ein Hilfsmittel zur Fehleranzeigeninterpretation in der Ultraschallprufung, Materialprufung, Nr. 6 (1976).
3. J. Schmolke, D. Hiller, H. Ermert, J. O. Schafer, G. Graber, Generation of Optimal Input Signals for Ultrasound Pulse-echo Systems, IEEE 1982 Ultrasonics Symposium, Symposium Proceedings Vol. 2 (1982).
4. G. Prokoph, H. Ermert, M. Kroning: A Broadband-Holography Imaging System for Nondestructive Evaluation, Acoustical Imaging, Vol. 15, (1986).
5. H. Ermert, R. Karg: Multifrequency Acoustic Holography, IEEE Trans. on Sonics and Ultrasonic, Vol. Su-26 (1979).
6. S. R. Doctor, F. E. Hall, L. D. Reid: SAFT-The Evolution of a Signal Processing Technology for Ultrasonic Testing, NDT International, Vol. 19, No. 3, (1986).